MECHANICS OF COHESIVE-FRICTIONAL MATERIALS, VOL. 2, 237–249 (1997)

Dilation characteristics of confined concrete

Amir Mirmiran[1]* and Mohsen Shahawy[2]

[1]*Department of Civil and Environmental Engineering, University of Central Florida, Orlando, FL 32816, U.S.A.*
[2]*Structural Research Center, Florida Department of Transportation, Tallahassee, FL 32310, U.S.A.*

SUMMARY

Confinement of concrete enhances its strength and ductility by restraining lateral dilation. The accuracy of a confinement model depends on how well it captures the dilation tendency of concrete. In recent years, external confinement of concrete by fibre composites has become increasingly popular for civil infrastructure applications. This includes fibre-wrapping of existing columns or encasement of concrete in a fibre reinforced plastics (FRP) shell. A total of 54-concrete-filled FRP tubes were tested in uniaxial compression under displacement control mode. Full instrumentation of the specimens has allowed the variation of tangent Poisson's ratio for concrete to be captured. The dilation trend of confined concrete is shown to be a function of jacket stiffness. In steel-encased members, once steel yields, confining pressure becomes constant and the jacket renders itself ineffective in containing the dilation of concrete. On the other hand, for linear-elastic materials such as fibre composites, a strain reversal occurs that results in containment of dilation. A method for predicting the dilation is developed that can be easily adopted in any active confinement model. Moreover, a new confinement model for FRP-encased concrete is discussed. © 1997 by John Wiley & Sons, Ltd.

Mech. Cohes.-Frict. Mater. **2**: 237–249 (1997)

No. of Figures: 11. No. of Tables: 2. No. of References: 21.

KEY WORDS: concrete; confinement; dilation; fibres; plastics

1. INTRODUCTION

Formation and growth of microcracks constitute a 'damage' process in concrete that is evidenced by its non-linear softening response under axial loads. The mode and extent of damage depends on the state of stress in the concrete member. Confinement in the form of discontinuous transverse reinforcement or full encasement is known to contain and delay the damage process by restraining the dilation of concrete.[1] The nature of such a confinement mechanism is passive in that the confining pressure is developed only after hoop elongation is imposed on the restraining member by Poisson's effect in concrete. In recent years, use of fibre composites in lieu of steel for confinement of concrete has been explored. Fibre-wrapping of existing columns has proved to be an effective retrofitting measure.[2] On the other hand, new hybrid systems have been developed by casting concrete in fibre reinforced plastics (FRP) tubes.[3] Confinement of concrete has been studied since the turn of this century.[4] Various constitutive models have been developed for constant active confining pressure[5] as well as passive confinement with steel hoops, spirals or tubes.[6,7] Investigators in the early 1990s attempted to apply the same models to fibre composites.[8] However, studies by the present authors[9]

*Correspondence to: A. Mirmiran, Department of Civil and Environmental Engineering, University of Central Florida, Orlando, FL 32816, U.S.A.

Contract sponsor: Florida and U.S. Deparments of Transportation

CCC 0271–2091/97/030237–13 $17.50

Received 5 July 1996
Revised 28 November 1996

and others[10] have shown that the behaviour of concrete encased in fibre composites is not fully captured by existing models. The effectiveness of confinement is measured by the enhancement in strength and ductility as a function of confining pressure. In a confinement mechanism, two conditions need to be satisfied; (1) geometric (strain) compatibility between the core and the confining member, and (2) equilibrium of forces in the free-body diagram for any sector of the confined section. The two conditions are interdependent, since the confining pressure is a function of lateral strains which in turn depends on the variation of Poisson's ratio for concrete.

In this paper, dilation characteristics of confined concrete are investigated by experimental methods and compared with analytical models. Although the thrust of this paper is directed towards linear-elastic confining members such as fibre composites, a discussion on the effect of type and stiffness of the restraining member on the dilation behaviour of confined concrete is also provided.

2. EXPERIMENTAL WORK

Florida Department of Transportation has sponsored a detailed study into the feasibility of using fibre composites for encasement of bridge pier columns and piles.[11] As part of this study, dilation characteristics of confined concrete were investigated using uniaxial compression tests on a total of 54 152.5 mm $\times$ 305 mm (6 in. $\times$ 12 in.) cylindrical specimens, of which 42 were made of concrete-filled glass fibre tubes, and 12 were control specimens (plain, unconfined concrete). All composite specimens consisted of a filament-wound angle-ply of polyester resin with unidirectional E-glass fibres at $\pm 15^\circ$ winding angle. The ultimate tensile strength of the fibres was given by the fibreglass manufacturer (CertainTeed Corporation, Fiber Glass Reinforcement, Wichita Falls, Texas) as 1 414 MPa (205 ksi) based on a split disc tensile test on a laminae containing 75.6% hoop fibres in an epoxy anhydride resin (DER 383/ECA 101). The percentage of fibres in the fibreglass tubes in this project was given by the fabricator as 63%–65%. In order to include the fibre fraction, fibre winding angle and the type of resin in the actual tubes used in the experiments, the classical laminate theory (CLT) was utilized.[12] Results were further verified by split disc tests of FRP rings.[13] Thicknesses of FRP tubes were indicated by the number of plies (or layers) of fibres. Six different thicknesses were tested (1.3, 1.9, 2.1, 3.0, 3.3 and 6.0 mm or 6, 9, 10, 14, 16 and 28 plies). Different concrete mixes with average strengths ranging between 20.7 MPa (3.0 ksi) and 46.9 MPa (6.8 ksi) were tested. Concrete slump varied between 50 mm (2 in.) and 127 mm (5 in.). All concrete mixes were made with Type II cement. Except for the first series with 12 specimens that were tested under a load control mode, all other specimens were loaded under a displacement control mode with a constant rate of 5.6 mm (0.22 in.) per minute. These specimens were also instrumented for measurement of axial and lateral strains of concrete and the tube. Both embedded strain gauges and surface rosettes were utilized. The embedded strain gauges were 30 mm long with 1 mm gauge width. The gauge was fitted by a string through two holes in opposite sides of the tube. Additionally, three LVDTs were used to measure the longitudinal displacements and average axial strains. Figure 1 shows the test set-up and instrumentation of one of the composite specimens. Figure 2 shows the typical failure modes for two of the concrete-filled FRP tubes with six plies. Details of experiments and instrumentation are reported elsewhere.[11] While the control specimens failed in a shear cone mode, for composite specimens, typical failure was generally marked by fracture of the fibreglass tube at or near the mid-height of the specimen. Failure near the top and bottom edges was not of consequence due to friction between the platens and the specimen. Failure, while sudden, was physically detectable and predictable. Sounds heard during the early-to-middle stages of loadings were attributed to the micro-cracking of concrete and shifting of aggregates. Snapping of the inner layers of the fibreglass could be heard near the end of the loading process. At about 60%–70% of the ultimate load, patches of white would begin to show near the mid-height of the tube. This indicated a plastic flow of the resin,

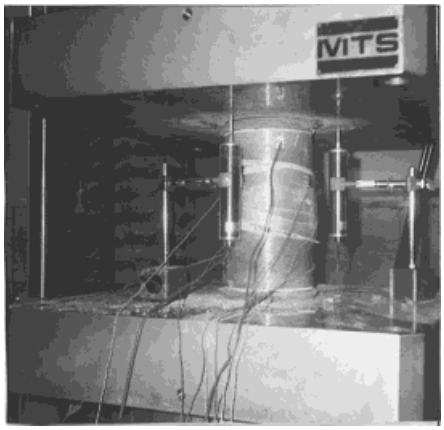

Figure 1. Instrumentation and test set-up

Figure 2. Typical failure for six-layer specimens

leaving only the white glass fibres to take the lateral load. The white patches would continue to grow towards the top and bottom edges. Although some local buckling and waving in the tubes were observed, shear failure was noted as the primary mode of failure for the tubes. It was also noted that specimens typically remained intact after failure.

3. ANALYSIS OF RESULTS

3.1. Stress–strain response

Typical stress–strain response for one of the FRP-encased series with 6, 10 and 14 layer tubes is shown in Figure 3. For each thickness, two specimens with the same properties were tested, and the figure shows consistency of the results. The curves to the right represent the plots of axial stresses versus axial strains, whereas the curves to the left show the plots of axial stresses versus lateral strains. Recent studies by Picher, Rochette and Labossière,[14] and Nanni and Bradford[10] have shown a similar response for fibre-wrapped columns with glass, kevlar and carbon fibres. By examining the stress–strain curves in Figure 3, the following observations are made.

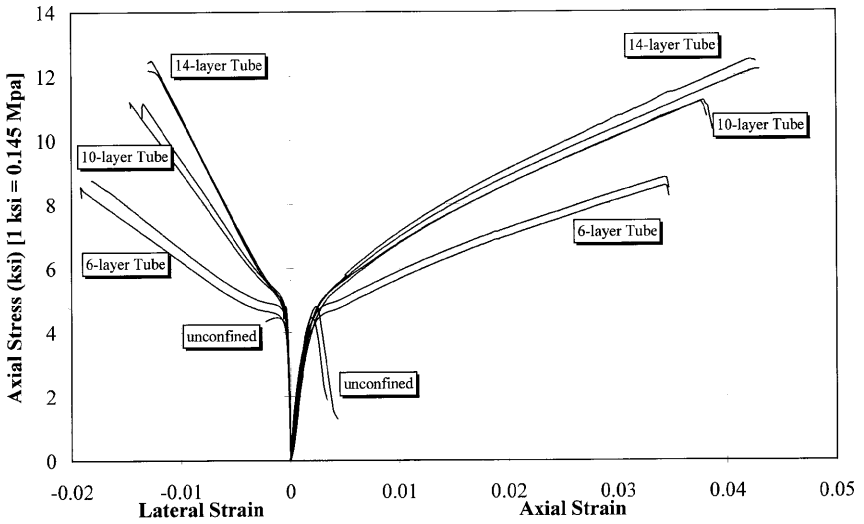

Figure 3. Stress–strain response for FRP-encased concrete

1. The figure clearly shows that confinement with FRP can significantly enhance concrete's performance, i.e., both strength and ductility. Confinement effectiveness for strength varies between two and three, depending on the jacket thickness. Confinement effectiveness is defined as the ratio of peak strength of confined concrete to that of unconfined concrete. Enhancement in ductility is more pronounced, as the ultimate strain of confined concrete is 10 to 15 times greater than that of plain (unconfined) concrete. Confinement effectiveness, however, is not a linear function of jacket thickness, as the difference between the 10 and 14 layer tubes is not as much as that between the six and 10 layer tubes.
2. Unlike steel-encased concrete, response of FRP-encased is bilinear with no descending branch. The bilinear trend is also confirmed by other investigators.[10,14] The response consists of three distinct regions. In the first region, behaviour is similar to plain concrete, since the lateral expansion of the core is insignificant. With the increase in microcracks, a transition zone is entered in which the tube exerts a lateral pressure on the core to counteract the core's tendency for stiffness degradation. Finally, a third region is recognized in which the tube is fully activated, and the stiffness is generally stabilized around a constant rate. The response in this region is mainly dependent on the stiffness of the tube.
3. Further investigation of the response shows a small softening area at the end of the transition zone. This is attributed to the straightening of unstretched filament-wound fibres once they become activated under internal pressure. An analogy can be drawn with the tensioning of a loose rope, which shows a soft response until it is stretched to its full straight and tight position. This behaviour is seen in both axial and lateral strains, especially for thinner jackets.
4. In the third region, response in the lateral direction is closer to a straight line than the response in the axial direction. This is due to excessive cracking of the concrete core which is no longer a homogeneous material. Therefore, lateral expansion of the specimen is directly dependent on the response of the jacket, which is linear-elastic. On the other hand, as the lateral cracks in the core expand, slight shifting and settling of the aggregates occur, whereby the specimen experiences mild softening in the axial direction. Ultimate failure is realized when the jacket can no longer carry any load. This occurs when the jacket fails in shear fracture mode.

3.2. Axial stress–volumetric strain

The true behaviour of confined concrete can be captured by examining its volumetric (volumic) stress–strain response. In a triaxial state of stress, volumetric strain ϵ_v (or dilatation) is defined as the volume change per unit volume:[15]

$$\epsilon_v = \epsilon_c + 2\epsilon_r \tag{1}$$

where, ϵ_c = axial strain and ϵ_r = lateral strain. Figure 4 shows plots of axial stress versus volumetric strain for one of the FRP-encased series with 6, 10 and 14 layers. For each thickness, two specimens with the same properties were tested, and the figure shows consistency of the results. A similar trend was observed for all other specimens in the test matrix. The confining pressure is calculated as below.

$$f_r = \frac{2f_j t_j}{D} = \frac{2E_j \epsilon_r t_j}{D} \tag{2}$$

where f_j = hoop stress in the jacket, E_j = modulus of elasticity of the jacket in the hoop direction, t_j = jacket thickness and D = core diameter. The response of plain concrete ($f_r = 0$) is similar to that observed by other researchers.[15] Initially, volume change is in the form of compaction and is almost linear up to the critical stress. At this point, direction of volume change is reversed, resulting in a volumetric expansion, called dilatancy, near or at peak strength. The expansion becomes unstable at the crushing phase of concrete. Tests by Kupfer, Hilsdorf and Rusch[16] and others[17,18] have shown that concrete behaves in the same manner under biaxial compression, although the critical stress and the volume reduction are both increased with lateral pressure. Similar investigations by Ahmad and Shah[7] and others have shown that volumetric strains of steel-encased concrete also become unstable after the steel casing yields. Figure 4 shows a unique characteristic for FRP-encased concrete. Initially, volume compaction occurs at a rate similar to the bulk modulus of the unconfined concrete. Owing to lateral pressure, however, the dilatancy phenomenon occurs at a higher stress and strain level than those of an unconfined concrete. The response shows a distinct point of maximum dilation

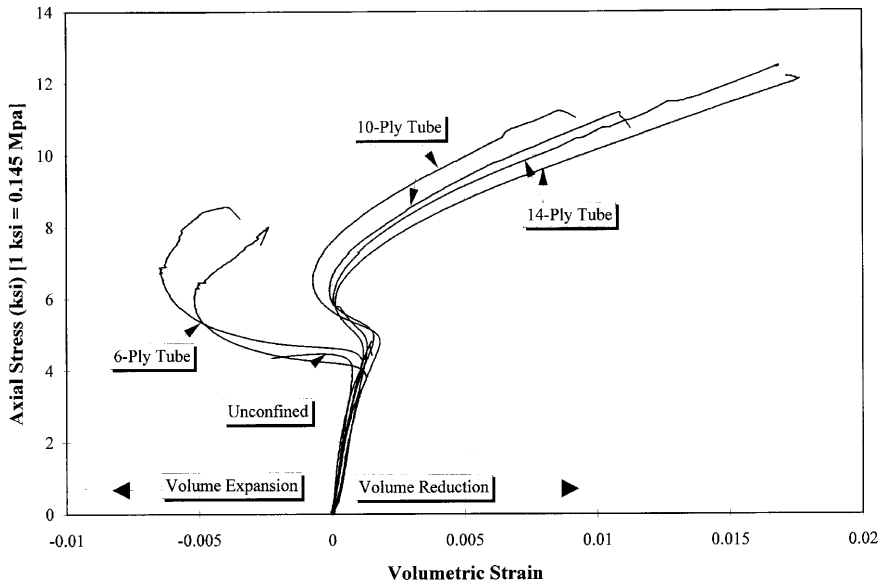

Figure 4. Axial stress–volumetric strain of FRP-encased concrete

where the second strain reversal occurs, and the dilatancy of concrete becomes contained. With an increase in the jacket thickness, one may expect to contain better the dilation phenomenon in concrete. For example, for the 14-layer FRP tube, effectively no dilation occurs. The volumetric response beyond the point of maximum dilation shows a linear trend that corresponds mainly to the hoop extension of the FRP tube. This dilation containment of FRP is better depicted by studying the Poisson's ratio for confined concrete.

3.3. Poisson's ratio and dilation rate

It is well known that the Poisson's ratio for concrete v remains in the range of 0.15 to 0.22, until approximately $0.7f'_c$, at which stress the *apparent* (or *secant*) *Poisson's ratio* (or strain ratio ϵ_r/ϵ_c) begins to increase. At the unstable crushing phase,[5] this ratio assumes values much higher than 0.5. Ottosen[19] proposed an elliptical variation for the strain ratio ($v = \epsilon_r/\epsilon_c$) as a function of plasticity index $\beta = f_c/f'_{cc}$, where f'_{cc} = confined strength of concrete, for $\beta > 0.8$. Another variation for Poisson's ratio has been suggested by Elwi and Murray[20] as a third degree polynomial in the form of:

$$v = v_0\left[1 + 1.3763\left(\frac{\epsilon_c}{\epsilon_{cr}}\right) - 5.36\left(\frac{\epsilon_c}{\epsilon_{cr}}\right)^2 + 8.586\left(\frac{\epsilon_c}{\epsilon_{cr}}\right)^3\right] \tag{3}$$

where ϵ_{cr} = critical strain of concrete. At a strain ratio of about 0.75, the value of v exceeds 0.5, which indicates the start of dilatancy. A better representation of the dilation characteristics of concrete is the tangent Poisson's ratio or the rate of change of radial (lateral) strains with respect to axial strains ($d\epsilon_r/d\epsilon_c$), which is herein termed as the dilation rate, μ. For the polynomial model proposed by Elwi and Murray,[20] the tangent and secant Poisson's ratios will behave similarly, with a higher rate of change for the latter. The dilatation rate for this model can be written as

$$\mu = \frac{d\epsilon_r}{d\epsilon_c} = v_0\left[1 + 2.7526\left(\frac{\epsilon_c}{\epsilon_{cr}}\right) - 16.08\left(\frac{\epsilon_c}{\epsilon_{cr}}\right)^2 + 34.344\left(\frac{\epsilon_c}{\epsilon_{cr}}\right)^3\right] \tag{4}$$

where the dilation rate exceeds 0.5 at a strain ratio of 0.49. Figure 5 shows a typical plot of dilation rate versus axial strain for one of the tested specimens with a 10-ply tube. The experimental dilation rate is calculated for every two consecutive readings as below:

$$\mu_{exp} = \frac{\Delta\epsilon_r}{\Delta\epsilon_c} = \frac{\epsilon_{r\,new} - \epsilon_{r\,old}}{\epsilon_{c\,new} - \epsilon_{c\,old}} \tag{5}$$

Note that the perturbations in the experimental dilation rate are due to the extensive number of readings per second, rather than the quality of the experimental results. In fact, if the number of data points kept is reduced, less perturbation will be seen. The solid line in the figure represents the dilation rate as the moving average of μ_{exp}. Also, one should note that the trend shown in the experimental curve has been consistent in all tested specimens, and can be captured by a fractional equation in the following form:

$$\mu = \frac{\mu_0 + ax + bx^2}{1 + cx + dx^2} \tag{6}$$

where μ_0 = initial dilation rate, $x = \epsilon_c/\epsilon_{co}$, ϵ_{co} = peak strain of unconfined concrete, and a, b, c and d are coefficients. The dilation curve shows three regions that generally correspond to those explained for the stress–strain response. First, the initial dilation rate (μ_0) is the same as the Poisson's ratio of unconfined concrete (v_0). As the microcracks develop, dilation rate tends to increase. The increase becomes more rapid at about $0.7\,f'_c$. Approaching the ultimate strain of unconfined concrete, where

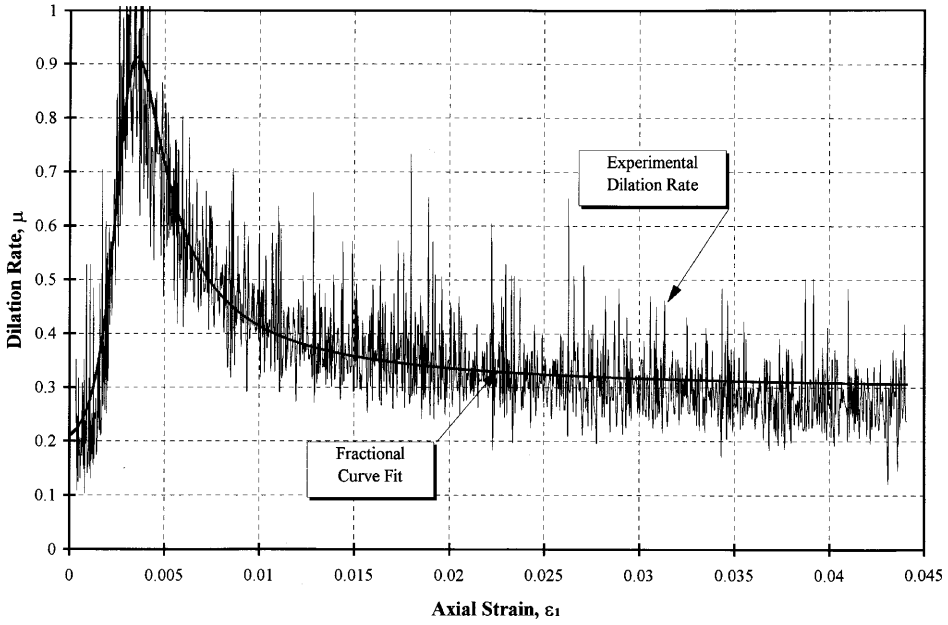

Figure 5. Typical dilation rate for FRP-encased concrete

concrete has lain itself entirely onto the jacket, the dilation rate reaches a peak value of μ_{max}. Once the jacket assumes full control of lateral expansion, dilation rate stabilizes and decreases to an asymptotic value of μ_u. A review of the properties of the dilation curve results in the following geometric constraints:

$$\begin{aligned} \mu(x=0) &= \mu_0, & \frac{d\mu}{dx}(x=0) &= 0 \\ \mu(x=1) &= \mu_{max}, & \frac{d\mu}{dx}(x=1) &= 0 \\ \mu(x\to\infty) &= \mu_u, & \frac{d\mu}{dx}(x\to\infty) &= 0 \end{aligned} \tag{7}$$

Upon imposing the above geometric constraints on the dilation curve, the four constants in equation (4) can be related to the initial peak and ultimate dilation rates as follows:

$$\begin{aligned} a &= \mu_0 c \\ b &= \mu_u d \\ c &= -2 \\ d &= \frac{\mu_{max} - \mu_0}{\mu_{max} - \mu_u} \end{aligned} \tag{8}$$

Figure 6 shows the dilation curves for various jacket thicknesses. As shown in the figure, the initial dilation rate μ_o only depends on the concrete core, whereas the peak and ultimate dilation rates depend on the stiffness of the jacket. As the thickness (or stiffness) of the tube increases, μ_{max} and μ_u both decrease. However, the decrease in μ_{max} in more pronounced than the decrease in μ_u. This indicates that thicker jackets contain the dilation of the concrete core sooner than their thin coun-

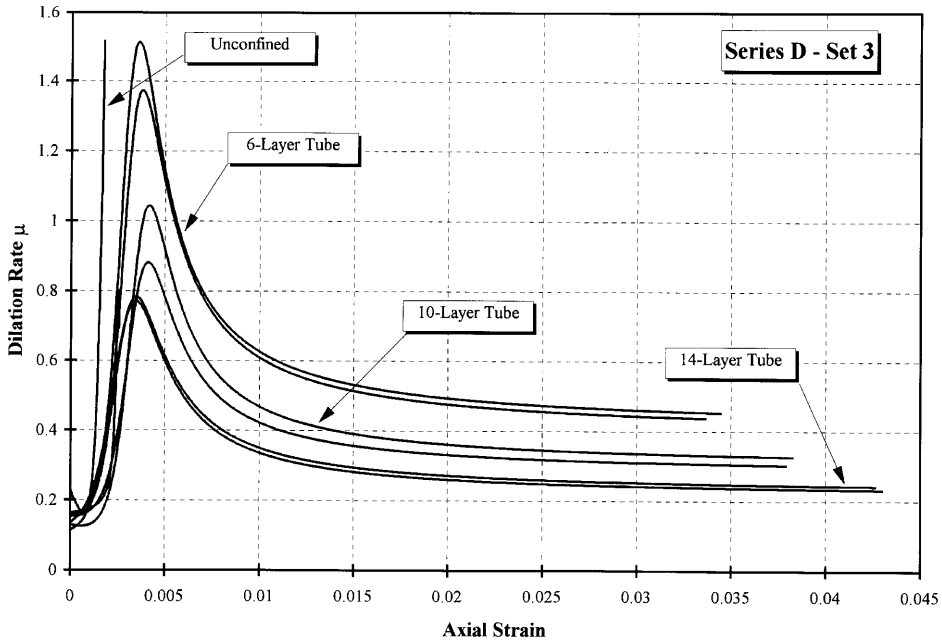

Figure 6. Effect of jacket thickness on dilation rates

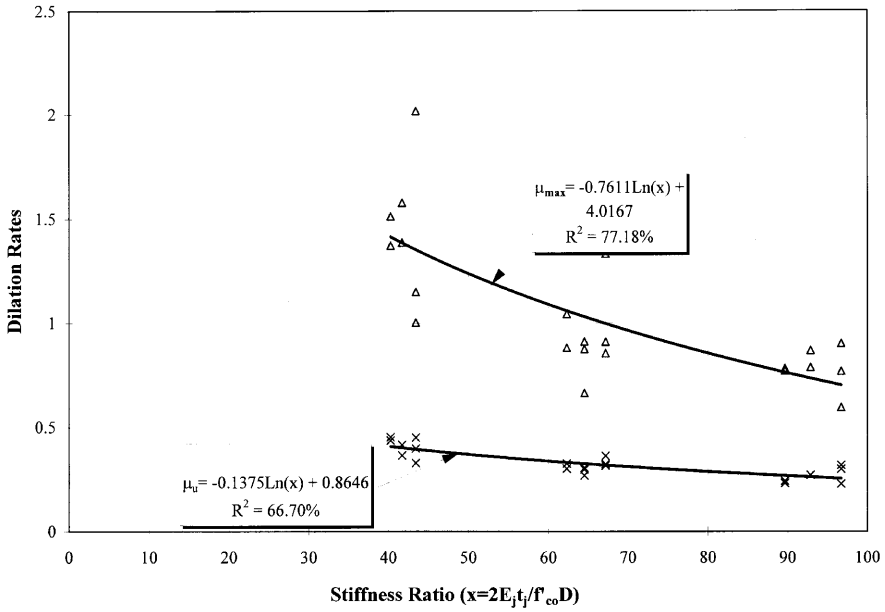

Figure 7. Effect of jacket stiffness on the peak and ultimate dilation rates

terparts. Figure 7 shows a cumulative plot of the peak and ultimate dilation rates, μ_{max} and μ_u, as functions of the stiffness ratio, which is defined as the stiffness of the jacket to that of the concrete core ($2E_j t_j/f'_{co}D$) where f'_{co} = strength of unconfined concrete. Since the modulus of concrete is often related to $\sqrt{f'_c}$, the denominator in the stiffness ratio is indicative of concrete strength as well as its stiffness. A logarithmic trend was observed between the values of dilation rate and the stiffness ratio. A regression analysis was made, and the following relationships were derived.:

$$\begin{aligned} \mu_{max} &= -0.7611\ \mathrm{Ln}\left(\frac{2E_j t_j}{f'_c D}\right) + 4.0167 \text{ with } (R^2 = 77.18\%) \\ \mu_u &= -0.1375\ \mathrm{Ln}\left(\frac{2E_j t_j}{f'_c D}\right) + 0.8646 \text{ with } (R^2 = 66.70\%) \end{aligned} \tag{9}$$

where Ln denotes the natural logarithm, and R^2 represents the statistical correlation. As shown in the figure, results for μ_{max} show more scatter than those for μ_u, which is evidenced by a lower coefficient of correlation (R^2). This may be attributed to the straightening of fibres in some of the tubes, as indicated in the discussion of stress–strain response. It should also be noted that the range of tested experiments included a stiffness ratio between 40 and 97.

3.4. Volumetric dilation rate

It is common to utilize the first derivative of strain invariants as the dilation rate. If I'_1 is the first strain invariant, and J'_2 is the second invariant of deviatoric strains, a volumetric dilation rate may be defined as

$$\Psi = \frac{\mathrm{d}I'_1}{\mathrm{d}\sqrt{J'_2}} = \frac{\mathrm{d}\epsilon_c + 2\ \mathrm{d}\epsilon_r}{\frac{1}{\sqrt{3}}(\mathrm{d}\epsilon_c - \mathrm{d}\epsilon_r)} \tag{10}$$

which can be related to the lateral dilation rate μ as below:

$$\Psi = \frac{1 + 2\mu}{\frac{1}{\sqrt{3}}(1 - \mu)} \tag{11}$$

Karabinis and Kiousis[21] assumed an exponential relation between the volumetric dilation rate and the confining pressure. Present study, however, indicates that both lateral and volumetric dilation rates are related to the confining pressure in a fractional form. Figure 8 shows a plot of dilation rates with respect to both axial and lateral strains. Since the material of the tube is linear-elastic, the same trend can be expected for the confining pressure. In the figure, the dilation rate μ is plotted as a negative value to signify the opposite directions of lateral and axial strains.

3.5. Comparison with steel-encased concrete

Based on the observed behaviour of FRP-encased concrete and prior investigations on plain (unconfined) and steel-encased concrete, dilation tendency of concrete is schematically shown in Figure 9. In this figure, normalized dilation rate (μ/μ_{cr}) is plotted against the axial strain of concrete, where μ_{cr} is defined as the critical dilation rate that may be the peak value for FRP-encased concrete, or the value of dilation rate at the onset of jacket yielding for steel-encased concrete. At the bottom half of the figure, normalized confining pressure (f_r/f_{ru}) is plotted against the axial strain of concrete. Curve *abd* shows the variation of dilation rate for plain concrete, which indicates an unstable dilation near ultimate strain. Curve *abcf* shows the variation of dilation rate for steel-encased concrete. At

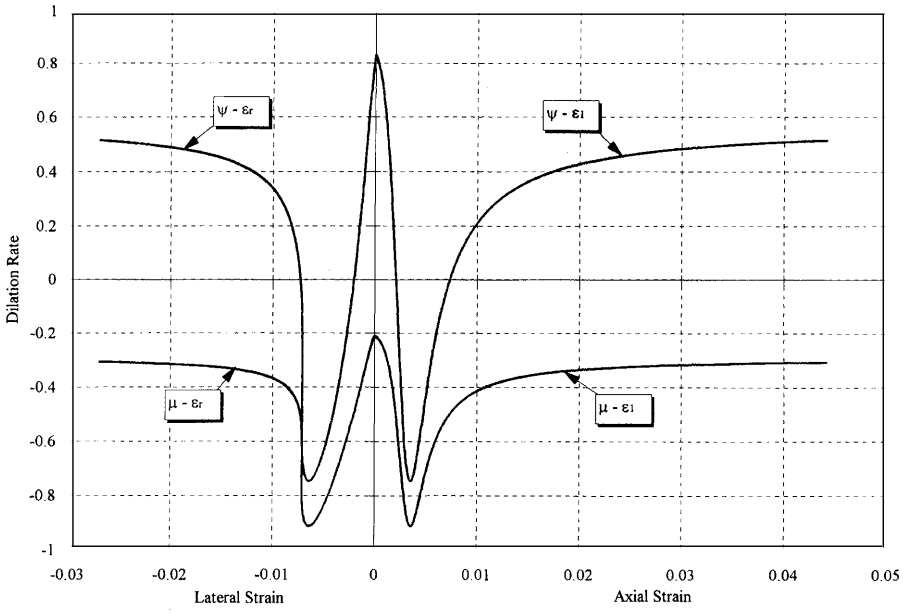

Figure 8. Lateral and volumetric dilation rates (μ and Ψ)

point *b*, the steel casing becomes activated and begins to contain the dilation of concrete core. However, with the yielding of steel at point *c*, an inflection occurs which results in the reversal of dilation curvature and its eventual instability at point *f*. Finally, curve *abceg* represents the variation of dilation rate for FRP-encased concrete. It follows the same pattern as steel-encased concrete to point *c*, where dilation rate decreases. At point *e* curvature of the dilation path changes and at some point *g* an asymptotic value of dilation rate is recognized.

4. CONFINEMENT MODELLING

Previous studies[9] have indicated that while most existing models produce accurate results for steel-encased concrete, they fall short of capturing the true response of FRP-encased concrete. This is attributed to their inability in estimating the dilatancy of confined concrete. When a steel jacket yields, the confining pressure becomes constant (see Figure 9) regardless of the variation of Poisson's ratio for concrete. On the other hand, for jackets made of linear-elastic material such as fibre composites, the accuracy of a confinement model depends on how well it can predict the dilation tendency of concrete. Based on the findings of the present study, a general confinement modelling technique is proposed that is applicable to both steel-encased and FRP-encased concrete. The schematic model is shown in Figure 10. For every axial strain ϵ_c, first the area under the corresponding dilation curve (upper left corner of the diagram) is calculated which corresponds to the lateral strain ϵ_r at the bottom right corner of the diagram. Then, based on the stress–strain relationship of the confining member (steel or FRP), the confining pressure f_r is determined (bottom left corner of the diagram). At this point, one can refer to any set of active confinement (constant pressure) curves (at the top right corner of the diagram), and determine the axial stress f_c that corresponds to the axial strain ϵ_c for the value of confining pressure f_r. This model has been shown to agree favourably with experimental results.[11] A more classical approach was also taken to represent a constitutive model for

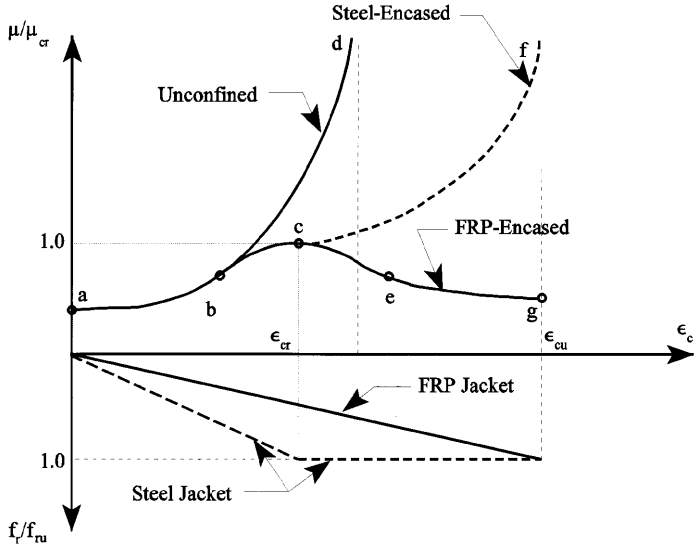

Figure 9. Schematic dilation curves for steel-encased and FRP-encased concrete

the FRP-encased concrete. Details of this approach are reported elsewhere.[11] Figure 11 shows a comparison of the proposed model with the experimental results.

5. CONCLUDING REMARKS

Full instrumentation of concrete-filled FRP tubes that were tested under uniaxial compression in a displacement control mode has revealed unique characteristics for FRP-encased concrete. Fibre composites, unlike steel, provide a linearly increasing confining pressure that can effectively contain the dilation tendency of concrete. On the other hand, in steel-encased concrete, once steel yields, the confining pressure becomes constant and the tube renders itself ineffective in containing the dilation. A dilation rate is defined as the tangent Poisson's ratio or the rate of change of lateral strains with

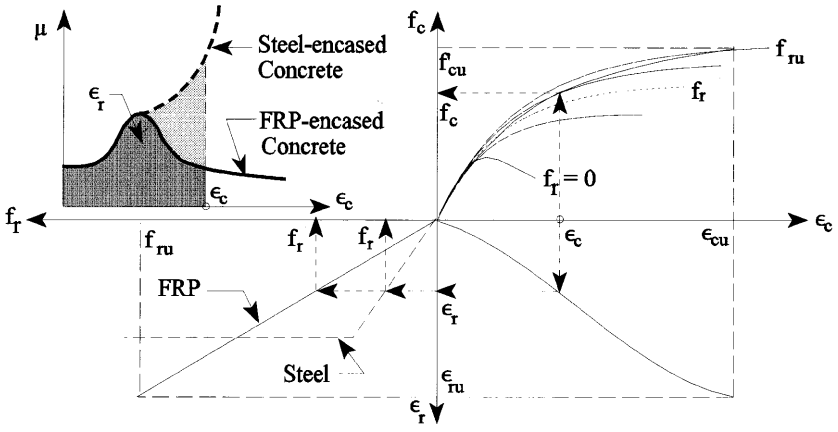

Figure 10. Schematic confinement modelling for FRP-encased concrete

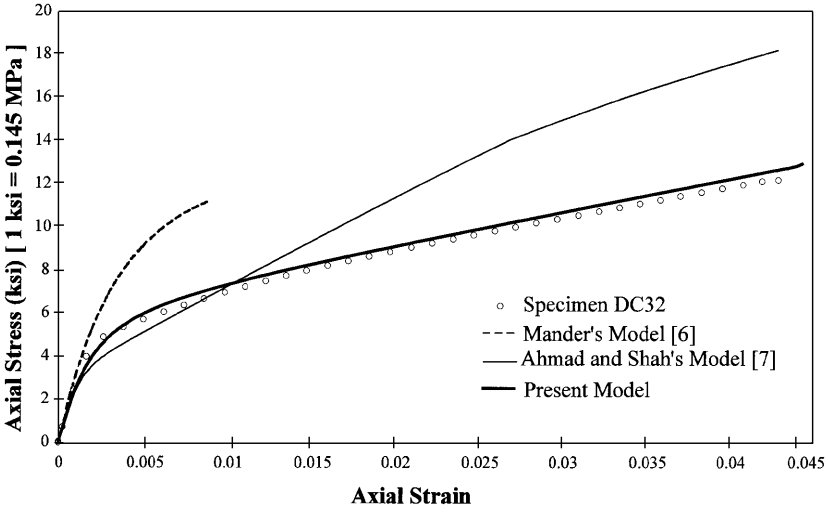

Figure 11. Comparison of confinement models for concrete-filled FRP tubes

respect to axial strains. It is shown that the dilation rate of FRP-encased concrete reaches a peak value which corresponds to a reversal in volumetric strain response. The dilation rate finally stabilizes at an ultimate value which is a function of the jacket's stiffness. A fractional equation is developed for the dilation response of FRP-encased concrete. The peak and ultimate dilation rates are related to a stiffness ratio which is defined as the ratio of jacket stiffness to that of the concrete core. Finally, it is shown that the proposed dilation model can be easily incorporated into any active confinement model.

ACKNOWLEDGEMENTS

Financial support for this study was provided by the Florida and the U.S. Departments of Transportation under WPI0510700, Contract No. B-9135. Materials for the tests were provided by Marine Muffler Corp., Orlando Paving Co. and Rinker Materials. The authors are grateful to the UCF graduate students: Michel Samaan. Mohsen Kargahi, Mike Scherer and Suramy Rodriguez for their diligent work on various aspects of the project. The opinions and findings expressed here, however, are those of the authors alone, and not necessarily the views of the sponsoring agencies.

REFERENCES

1. K. Newman and J. B. Newman, 'Failure theories and design criteria for plain concrete', *Proc. Int. Civil Eng. Mater. Conf. on Struct., Solid Mech. and Eng. Design*, Wiley Interscience, New York, NY, pp. 936–995, 1971.
2. M. J. N. Priestley, F. Seible and M. Calvi, *Seismic Design and Retrofit of Bridges*, John Wiley & Sons, New York, NY, 1995.
3. A. Mirmiran and M. Shahawy, 'A novel FRP-concrete composite construction for the infrastructure', *Proc. 13th Structures Congress*, Boston, MA, ASCE, pp. 1663–1666, 1995.
4. A. Considirè, *Experimental Researches Reinforced Concrete*, English translation by L. F. Moisseiff, McGraw-Hill Book Co., New York, NY 1903.
5. F. E. Richart, A. Brandtzag and R. L. Brown, 'A study of the failure of concrete under combined compressive stresses', *Engineering Experiment Station Bulletin No. 185, University of Illinois, Urbana, IL, 1928.*
6. J. B. Mander, M. J. N. Priestley and R. J. T. Park, 'Theoretical stress–strain model for confined concrete', *J. Struct. Eng.*, **114**, 1804–1826 (1988).

7. S. H. Ahmad and S. P. Shah, 'Complete triaxial stress–strain curves for concrete', *J. Struct. Eng.*, **108**, 728–742 (1982).
8. H. Saadatmanesh, M. R. Ehsani and M. W. Li, 'Behavior of externally confined concrete columns', *Proc. Int. Symp. on Fiber-Reinforced-Plastic reinforcement for Concr. Struct.*, eds. A. Nanni and C. W. Dolan, ACI, SP 138, pp. 249–265, 1993.
9. A. Mirmiran, M. Kargahi, M. S. Samaan and M. Shahawy, 'Composite FRP-concrete column with bi-directional external reinforcement', *Proc. 1st Int. Conf. Composites in Intrastructure*, eds. H. Saadatmanesh and M. R. Ehsani, Tucson, AZ. pp. 888–902, 1996.
10. A. Nanni and M. N. Bradford, 'FRP jacketed concrete under uniaxial compression', *Constr. & Bldg. Materials*, **9**, 115–124 (1995).
11. A. Mirmiran, 'Analytical and experimental investigation of reinforced concrete columns encased in fibreglass tubular jackets and use of fiber jacket for pile splicing', *Final Report*, WPI 0510700, Contract No. B-9135, Florida Department of Transportation, Tallahassee, FL, 1996.
12. M. Kargahi, 'Fiber reinforced plastic (FRP) shell as external reinforcement for concrete columns', *M.S. Thesis*, University of Central Florida, Orlando, FL, 1995.
13. M. Scherer, 'Design optimization and behavior of concrete-filled FRP tubes', *M.S. Thesis, University of Central Florida, Orlando, FL, 1996.*
14. F. Picher, P. Rochette and P. Labossière, 'Confinement of concrete cylinders with CFRP', *Proc. 1st Int. Conf. Composites in Infrastructure*, eds. H. Saadatmanesh and M. R. Ehsani, Tucson, AZ, pp. 829–841, 1996.
15. W. F. Chen, *Plasticity in Reinforced Concrete*, McGraw-Hill Book Co., New York, NY, 1982.
16. H. Kupfer, H. K. Hilsdorf and H. Rusch, 'Behavior of concrete under biaxial stresses', *ACI J.* , **66**, 656–666 (1969).
17. L. Cedolin, Y. R. J. Crutzen and S. D. Poli, 'Traxial stress-strain relationship for concrete', *J. Eng. Mech.*, **103**, 423–439 (1977).
18. K. H. Gerstle, *et al.*, 'Behavior of concrete under multiaxial stress states', *J. Eng. Mech.*, **106**, 1383–1403 (1980).
19. N. S. Ottosen, 'Constitutive model for short-time loading of concrete', *J. Eng. Mech.*, **105**, 127–141 (1979).
20. A. A. Elwi and D. W. Murray, 'A 3D hypoelastic concrete constitutive relationship', *J. Eng. Mech.*, **105**, 623–641 (1979).
21. A. I. Karabinis and P. D. Kiousis, 'Effects of confinement on concrete columns: plasticity approach', *J. Struct. Eng.*, **120**, 2747–2767 (1994).

